



Multi-amplitude voltage vector MPTC for dual three-phase PMSMs with low torque ripple

Shuang Wang¹ · Qianru Zhang¹ · Deliang Wu¹ · Jianfei Zhao¹

Received: 22 March 2023 / Revised: 31 July 2023 / Accepted: 1 August 2023 / Published online: 10 August 2023
© The Author(s) under exclusive licence to The Korean Institute of Power Electronics 2023

Abstract

In model predictive torque control (MPTC), voltage vectors with a fixed amplitude have poor performance in torque tracking. In this paper, a multi-amplitude MPTC (MA-MPTC) method for dual three-phase permanent magnet synchronous motor (PMSM) is proposed, which can effectively reduce torque ripple by combining virtual voltage vectors (VVs) and actual voltage vectors (AVVs). First, the deadbeat (DB) technique is used to simplify voltage vector selection and to avoid the enumeration of all the possible voltage vectors. After calculating the reference voltage vector (RVV) using this method, four vectors with different amplitudes can be selected as candidate voltage vectors (CVVs) according to the angle of the RVV. Then a new cost function is used to calculate the four candidate vectors, and the vector that minimizes the cost function is the optimal vector. Therefore, the MA-MPTC strategy has the advantages of both the MPTC method and the DB method, which can effectively reduce the torque ripple with a low computational cost. In addition, VVs are used to reduce the influence of harmonic currents while suppressing torque ripple. Finally, the stability and dynamic response are investigated on the test bench. When compared with a contrast method, the torque ripple is reduced by nearly half and the advantage of fast response is maintained. The experimental results confirm the effectiveness of the proposed method.

Keywords Dual three-phase permanent magnet synchronous motor · Virtual voltage vector · Torque ripple · Model predictive torque control

1 Introduction

With advances in motor drive technology, the multiphase permanent magnet synchronous motor (PMSM) has become a competitive choice for high power applications that require high reliability. Due to their distinct advantages of lower torque ripple at low speeds, better fault tolerance, and greater control freedom [1], multiphase machines have been widely used in electric cars, aerospace, and medical equipment [2, 3]. Meanwhile the control of dual three-phase PMSMs have been extensively researched. This research includes field-oriented control [4], direct torque control [5] and model predictive control (MPC) [6]. In particular, MPC is widely used in the field of power system [7, 8], and has received an increasing amount of attention in the field of motor control [9]. This is due to the fact that it offers several advantages,

such as simple implementation, short response time, and flexible control of nonlinear parameters.

One of the characteristics of dual three-phase PMSMs is that there are inherently no sixth-order harmonics associated with the torque ripple [10]. However, due to the problem of inverter nonlinearity and the presence of low leakage inductance in the windings, a large number of harmonic currents are generated in the x - y subspace. To solve this problem, an MPC method based on a disturbance observer was proposed in [11], which effectively suppressed low-order harmonics. However, the design and computation of the observer make the algorithm particularly complex, due to the large number of parameter calculations. A new control strategy using MPC for the control of a wind turbine system was introduced in [12], which was based on a permanent magnet synchronous generator. This strategy uses a voltage control loop for the voltage source inverter to reduce the THD of the grid currents. In [13], the harmonic current can be reduced to some extent by selecting appropriate vectors based on the position of the flux linkage in the x - y subspace. However,

✉ Jianfei Zhao
jfzhao@shu.edu.cn

¹ School of Mechatronic Engineering and Automation, Shanghai University, Shanghai, China

the range of candidate voltage vectors (CVV) is so large that it is difficult to select a vector that provides the best control.

To further suppress harmonics, 12 VVVs were synthesized by combining the characteristics of 24 actual voltage vectors (AVVs) at the periphery [14]–[16]. The amplitude of the VVVs in x – y subspace is 0, which means that the harmonic current in the x – y subspace is theoretically eliminated and can achieve good performance in reducing current harmonics. At present, the study of VVVs is very extensive. In [17], power fluctuations and harmonic currents were suppressed, and the complexity of the algorithm was reduced. In [18], a combination of model-free MPC and VVVs was proposed to control the fundamental and harmonic currents to improve the control performance under the conditions of uncertain motor parameters. However, the methods discussed above only focus on the harmonic suppression problem, while torque ripple suppression is not considered. Reducing the torque ripple is a more important issue to consider when it comes to improving motor control performance.

Usually, model predictive torque control (MPTC) uses a cost function that includes a flux linkage error and a torque error to suppress torque ripple [19]. Unfortunately, torque ripple increases when VVVs are applied because VVVs have a common amplitude value and the torque cannot be flexibly adjusted. In [20, 21], a fixed duty cycle method was introduced to alleviate this problem. In [20], discrete space-vector modulation was proposed in VVVs based vector space to generate more voltage vectors to generate CVVs with different amplitudes. Then the newly constructed set of CVVs was directly screened by a cost function. In [21], the range of the optimal voltage vector was gradually reduced by computing a cost function three times after synthesizing voltage vectors with different phases and amplitudes. Considering the harmonic problem, a hybrid control set combining virtual voltage vector and duty ratio control was designed in [22], which can both suppress harmonic current and improve torque control performance. However, this complicates the MPC algorithm, and the fixed duty ratio increases the number of candidate voltage vectors, which increases the computational burden of the control system. In addition, the main disadvantage of a fixed duty is that the torque cannot be accurately adjusted, which limits the suppression of torque ripple. Therefore, the torque error increases a fairly large amount.

By calculating the duty of the effective voltage vector according to different control objectives, more precise torque control can be achieved [23, 24]. After obtaining the optimal voltage vector, the duty cycle of the vector is calculated according to the principle of deadbeat tracking to reduce the tracking error of the system [23]. In [24], based on the principle of torque ripple minimization, the duty of the action voltage vector is obtained to

reduce the torque ripple and harmonic content in the stator current without reducing the dynamic performance. This method is more flexible in controlling torque ripple. However, it has a high computational cost. Algorithms combining VVVs with multi-vector MPTC were studied in [25, 26]. The voltage vector with the optimal phase is obtained by means of the stator flux amplitude reaching its reference value, and the duty of the optimal vector is optimized according to the principle of minimum torque error to reduce the ripple of torque and flux [25]. In [26], a fault-tolerant MPTC method based on deadbeat control was presented. Under the fault condition, VVVs were used as CVVs. The deadbeat is used to predict the RVV, and the optimal VVV is quickly selected, which reduces the calculation burden and improves the steady-state performance.

After determining the optimal VVV, the action time of the selected VVV is obtained by geometric principle. The multi-vector control method improves the steady-state performance. However, the duty circle determination method is complicated. When compared with these methods, the proposed method realizes multi-amplitude control by introducing voltage vectors with different amplitudes. The calculation of the duty ratio is simplified while the torque ripple is suppressed. In addition, determining the reference voltage vector has been shown to be a good way to reduce the computational cost [27, 28]. Depending on the sector in which the RVV is located, vectors whose actions are most similar to the RVV can be selected as prediction vectors, which reduces the torque ripple.

In this paper, a multi-amplitude MPTC method (MA-MPTC) with a low torque ripple that is capable of reducing harmonic currents and computational complexity is proposed. After calculating the amplitude and phase of the RVV, two voltage vectors of the outer layer and VVVs with different amplitudes (36 voltage vectors in total) are considered. Then one null vector and the three in-phase vectors closest to the RVV are selected as CVVs. In this way, the number of CVVs can be reduced to 4. Then a novel cost function consisting of the x – y subspace current and the error between the magnitude of the RVV and the CVVs is designed. Moreover, in this paper, a fixed switching frequency is achieved by three methods, including inserting a null vector, adjusting the actual vector action sequence, and replacing two-vector synthesis with three-vector synthesis. Finally, the effectiveness of the MA-MPTC is verified by the experimental results.

The contribution of this paper can be summarized as follows.

- (1) A multi-amplitude MPTC method for dual three-phase permanent magnet synchronous motor systems is proposed.

- (2) Constructing candidate voltage vectors with different amplitudes can reduce torque ripple, which makes it possible to avoid complicated duty ratio calculations.
- (3) The reference voltage vector is used to reduce the number of candidate voltage vectors, which further reduces the complexity of the algorithm.
- (4) A new cost function consisting of the x - y subspace current and the error between the magnitude of the RVV and the CVVs is designed, which considers both the control of the torque and the harmonic current.

2 Mathematical model

A dual three-phase PMSM is fed by a two-level voltage source inverter (VSI), as shown in Fig. 1. Each of the switching states defines an actual voltage vector in the α - β subspaces and the x - y subspaces, as shown in Fig. 2. The directions of L_1 , L_3 and L_4 vector groups are the same, and the L_2 vector group is 15 degrees apart from them. The same set of voltage vectors are separated by 30 degrees each. In Fig. 2a, the α - β subspace is divided into twelve sectors, which are indicated by the symbols Q_1, Q_2, \dots, Q_{12} .

Based on the coordinate transformation of vector space decomposition (VSD) [29], the voltage, flux linkage and torque equations in the d - q subspace can be described as formula (1) through formula (3).

$$\begin{cases} u_d = Ri_d + \frac{d\psi_d}{dt} - \omega_e \psi_q \\ u_q = Ri_q + \frac{d\psi_q}{dt} + \omega_e \psi_d \end{cases} \quad (1)$$

$$\begin{cases} \psi_d = L_d i_d + \psi_f \\ \psi_q = L_q i_q \end{cases} \quad (2)$$

$$T_e = 3p(\psi_d i_q - \psi_q i_d) \quad (3)$$

where $u_d, u_q, i_d, i_q, L_d, L_q, \psi_d,$ and ψ_q are the stator voltage, current, inductance, and flux in the d - q axis; ω_e is the

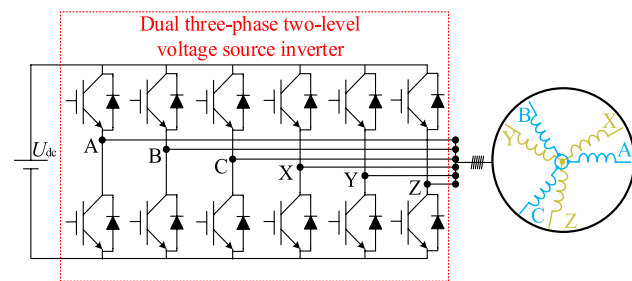


Fig. 1 Dual three-phase PMSM electric drive system

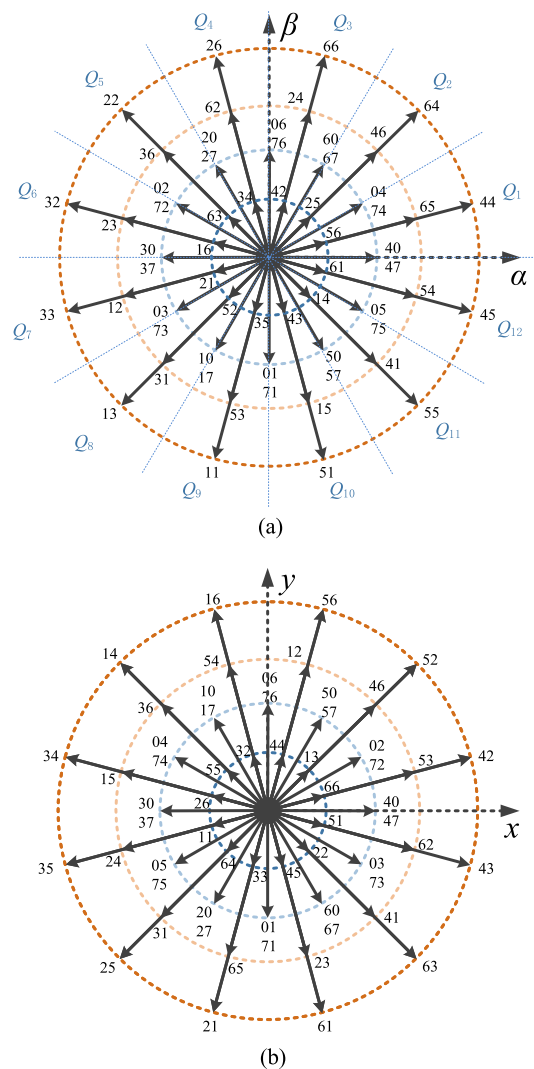


Fig. 2 Voltage vectors in the: **a** α - β subspace; **b** x - y subspace

electrical angular speed of the rotor; ψ_f is the permanent magnet flux linkage; T_e is the electromagnetic torque; R is the stator resistance; and p is the number of pole pairs.

3 Torque ripple analysis

Using the forward Euler approximation method in [30], the discrete model of the motor in the d - q coordinate is represented as follows:

$$\begin{cases} \psi_d(k+2) = \psi_d(k+1) + u_d(k+1)T_s \\ \quad + \omega_e \psi_q(k+1)T_s - Ri_d(k+1)T_s \\ \psi_q(k+2) = \psi_q(k+1) + u_q(k+1)T_s \\ \quad - \omega_e \psi_d(k+1)T_s - Ri_q(k+1)T_s \end{cases} \quad (4)$$

$$\begin{cases} i_d(k+2) = \left(1 - \frac{T_s R}{L_d}\right) i_d(k+1) \\ \quad + \frac{L_q}{L_d} T_s \omega_e i_q(k+1) + \frac{T_s}{L_d} u_d(k+1) \\ i_q(k+2) = \left(1 - \frac{T_s R}{L_q}\right) i_q(k+1) - \frac{T_s \omega_e \psi_f}{L_q} \\ \quad + \frac{T_s}{L_q} u_q(k+1) - \frac{L_d}{L_q} T_s \omega_e i_d(k+1) \end{cases} \quad (5)$$

where T_s is the control period.

By differentiating both sides of (3), the state equation of the electromagnetic torque is obtained as:

$$\dot{T}_e = 3p \left(\dot{\psi}_d i_q + \psi_d \dot{i}_q - \dot{\psi}_q i_d - \psi_q \dot{i}_d \right) \quad (6)$$

Substitute formulas (4) and (5) into (6), the voltage vector in the d - q coordinate can be described as:

$$u_q(k+1)T_s = M u_d(k+1) + B \quad (7)$$

For the dual three-phase PMSM studied in this paper, $L_d = L_q$, where:

$$M = 0 \quad (8)$$

$$B = \frac{L_d [T_e(k+2) - T_e(k+1)]}{3p\psi_f} + T_s \omega_e L_d i_d(k+1) + RT_s i_q(k+1) + T_s \omega_e L_d \psi_f \quad (9)$$

For more accurate torque tracking, the electromagnetic torque reference T_e^{ref} should suffice:

$$T_e(k+2) = T_e^{ref} \quad (10)$$

where T_e^{ref} is the reference of the torque.

If $u_d(k+1)T_s - u_q(k+1)T_s$ are taken as coordinate axes, the expression of the torque can be represented as a straight line, as shown in Fig. 3 [31]. The vectors falling on this line can realize the deadbeat tracking of the torque.

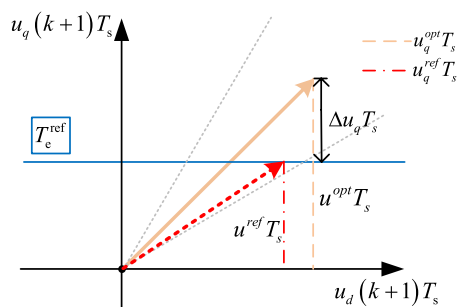


Fig. 3 Torque ripple analysis

With (7), the predictive torque can be described as:

$$T_e(k+2) = T_e(k+1) + \frac{3p\psi_f}{L_d} [-T_s \omega_e L_d i_d(k+1) - T_s \omega_e L_d \psi_f - RT_s i_q(k+1) + u_q(k+1)T_s] \quad (11)$$

The torque ripple is due to the difference between the predicted torques of the CVV and the RVV. Therefore, the torque ripple can be expressed as follows:

$$\Delta T_e = \frac{3p\psi_f}{L_d} \Delta u_q T_s \quad (12)$$

where $\Delta u_q = u_q^{opt} - u_q^{ref}$ represents the difference in the q -axis component between the two voltage vectors; u_q^{opt} is the q -axis component of the CVV; u_q^{ref} is the q -axis component of the RVV; and ΔT_e represents the torque error caused by the two vectors.

As shown in Fig. 3, u^{ref} is the RVV and u^{opt} is the CVV. The larger Δu_q is, the larger the torque tracking error is. However, if vectors of the same amplitude are used, the torque tracking error is fixed in the same sector and cannot be flexibly adjusted. Therefore, by increasing candidate vectors with different amplitudes, the vector whose q -axis voltage difference between the candidate vector and the RVV is reduced, and the torque error is reduced. However, 12 CVVs must be added for each new amplitude value, which results in a high computational cost.

4 Proposed MPTC method

4.1 RVV calculation

The proposed MPTC strategy is shown in Fig. 4. According to the deadbeat predictive control in [32], the RVV can be calculated by:

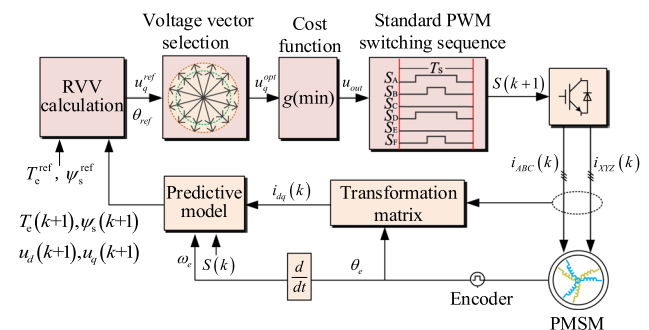


Fig. 4 Control diagram of the MA-MPTC method

$$T_s^2 u_d^2(k+1) + 2\psi_d(k+1)T_s u_d(k+1) + [\psi_d^2(k+1) + (\psi_q(k+1) + B)^2 - (\psi_s^{ref})^2] = 0 \tag{13}$$

Thus:

$$u_d(k+1) = \frac{-b \pm \sqrt{b^2 - 4ac}}{2a} \tag{14}$$

where Ψ_s^{ref} is the reference of the stator flux:

$$\begin{cases} a = T_s^2 \\ b = 2\psi_d(k+1)T_s \\ c = \psi_d^2(k+1) + [\psi_q(k+1) + B]^2 - (\psi_s^{ref})^2 \end{cases} \tag{15}$$

u_q of the RVV can be calculated by formula (7).

$$u_q(k+1) = \frac{B}{T_s} \tag{16}$$

The angle of the RVV in the α - β subspace can be calculated by:

$$\theta^{ref}(k+1) = \arctan \frac{u_\beta(k+1)}{u_\alpha(k+1)} \tag{17}$$

4.2 Optimal vector selection

From Fig. 2, it can be seen that the L_1 group vectors have a large amplitude in the x - y subspace and that the L_2 group vectors have a large angular deviation from the RVV. Thus, the L_1 and L_2 group vectors are not suitable to be CVVs. On the other hand, the voltage vectors of the L_3 and L_4 groups have the same direction in the α - β subspace but opposite directions in the x - y subspace. Therefore, the voltage vectors of the L_3 and L_4 groups in the α - β subspace can be synthesized to obtain a set of VVVs (uu_1 - uu_{12}) whose amplitude is 0 in the x - y subspace. The specific distribution is shown in Fig. 2, which is called the G group. In addition, the magnitude of the VVVs in the α - β subspace is $0.597 U_{dc}$, and the action times of the actual vectors from the group L_4 and the group L_3 are $0.731 T_s$ and $0.269 T_s$, respectively.

In summary, the CVVs are composed of voltage vectors of the groups L_3 , L_4 , and G along with null vectors, as illustrated in Fig. 5. It can be seen that regardless of which sector the RVV is located, 4 voltage vectors with different amplitudes can be selected, which reduces the torque ripple caused by the fixed amplitude.

Since the four CVVs have the same phase but different amplitudes, a novel cost function is developed, which is the difference between the magnitude of the RVV and the four

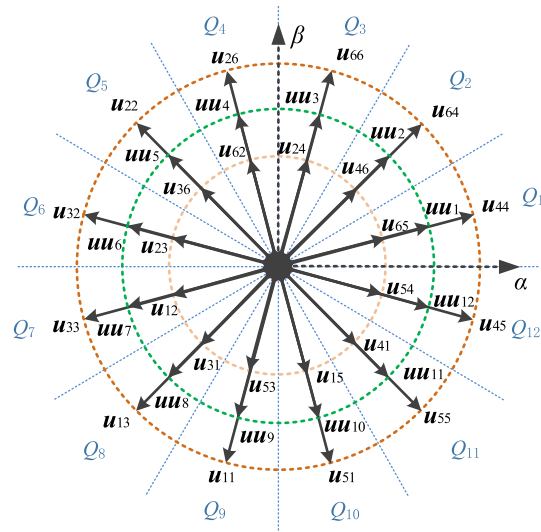


Fig. 5 CVV map

CVVs, taking into account the suppression of the x - y subspace currents. The cost function is expressed as follows:

$$g = \left| \mathbf{u}_q^{ref} \right| - \left| \mathbf{u}_q^{opt} \right| + \lambda \left(\left| i_x(k+2) \right| + \left| i_y(k+2) \right| \right) \tag{18}$$

where $\lambda > 0$; $|\mathbf{u}_q^{opt}|$ is the amplitude of the CVV in the q axis; and $i_x(k+2)$ and $i_y(k+2)$ are the predicted values of the harmonic current at the instant $k+2$, which can be calculated according to (19).

$$\begin{cases} i_x(k+2) = \frac{(1-T_s R)i_x(k+1) + T_s u_x(k+1)}{L_i} \\ i_y(k+2) = \frac{(1-T_s R)i_y(k+1) + T_s u_y(k+1)}{L_i} \end{cases} \tag{19}$$

where $u_x(k+1)$ and $u_y(k+1)$ are the stator voltage in the x - y subspace at the instant $k+1$.

4.3 Switching pulse generation

To facilitate digital control, the inverter input signal usually takes the form of a standard PWM sequence. In this paper, the switching pulse sequence is standardized based on SVPWM modulation with seven segments. For group G , there are two actual effective voltage vectors that must act in one control cycle. In addition, half of the vectors in group G cannot implement standard PWM pulses in one period.

According to this property, the 12 virtual vectors of group G can be divided into 2 groups: G_1 ($uu_1, uu_3, uu_5, uu_7, uu_9, uu_{11}$) and G_2 ($uu_2, uu_4, uu_6, uu_8, uu_{10}, uu_{12}$).

For group G_1 , the action sequence of the effective voltage vector is adjusted in one control cycle. Then null vectors are inserted to standardize the switching pulse sequence of VVV

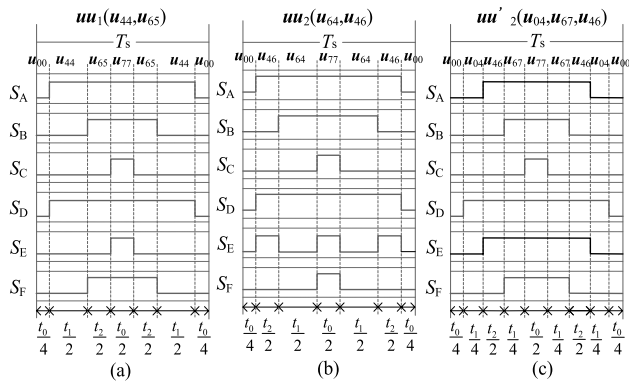


Fig. 6 Switching pulses generation for various virtual vectors: a uu_1 ; b uu_2 ; c uu'_2

in group G_1 . As shown in Fig. 6a, these are the standard PWM switching sequences of uu_1 .

For group G_2 , the standard PWM pulse cannot be generated regardless of how the action sequence of the voltage vectors changes as shown in Fig. 6b. Similar problems also occur for the switching pulse sequences of the other vectors in group G_2 . The method used in this work is to replace the voltage vectors of group L_4 with two voltage vectors of group L_2 [11]. For example, the VVV uu_2 is equal to the virtual vector synthesized by u_{46} , u_{04} , and u_{67} (denoted as v_2). From Fig. 6c, the vector v_2 can represent a standard PWM switching sequence. For group G_2 , the action times of the vectors of groups L_2 and L_3 are t_3 and t_4 , which can be calculated as follows:

$$\begin{cases} 2t_3 + t_4 = t_{out} \\ 0.173U_{DC} \cdot t_3 - 0.471U_{DC} \cdot t_4 = 0 \end{cases} \quad (20)$$

By (20), t_3 is $0.4223 t_{out}$ and t_4 is $0.1554 t_{out}$.

A flow diagram of the method proposed in this paper is shown in Fig. 7.

In general, the main idea of MA-MPTC is to use vectors with different amplitudes to reduce the torque ripple. Then the RVV is used to reduce the set of candidate vectors, which reduces the computational cost.

5 Experimental performance results

The experimental bench used in this paper is shown in Fig. 8, and the load is a servo motor. In the following, the performances of the MPTC method based on VVVs (MPTC1) and the MA-MPTC are compared. The parameters of the experimental bench can be found in Table 1. Figure 8 and Fig. 9 show the steady state performance of MPTC1 and MA-MPTC at a speed of 100 rpm. The load torque is set to 3 N·m and 5 N·m, respectively.

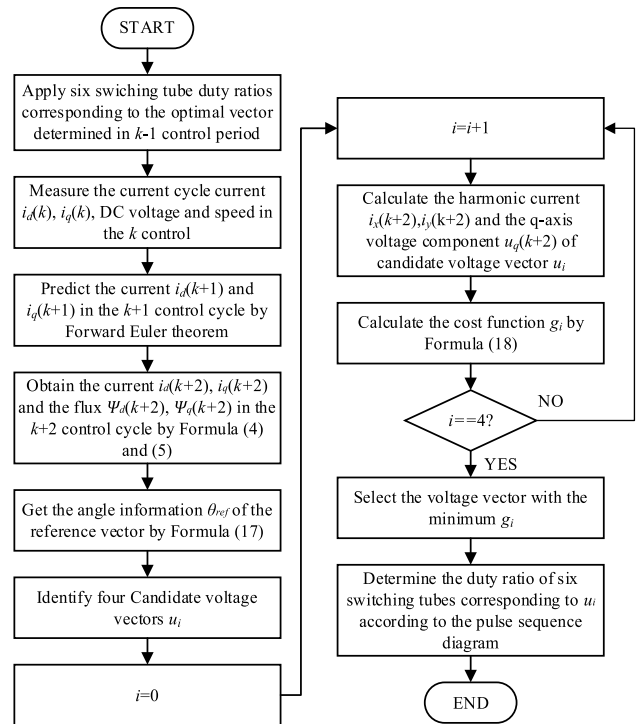


Fig. 7 Flow diagram of the proposed method

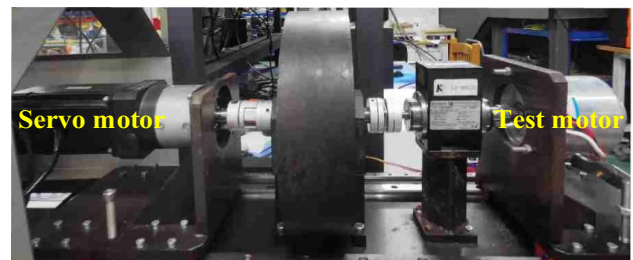


Fig. 8 Test bench

Table 1 Experimental motor parameters

| Specification | Value |
|-------------------------------|--------|
| Rated torque(N·m) | 5 |
| Rated current(A) | 60 |
| Number of pole pairs | 5 |
| Stator resistance(Ω) | 0.0225 |
| d-axis inductance(mH) | 0.053 |
| q-axis inductance(mH) | 0.053 |
| Stator leakage inductance(mH) | 0.0027 |
| Stator flux(Wb) | 0.0056 |

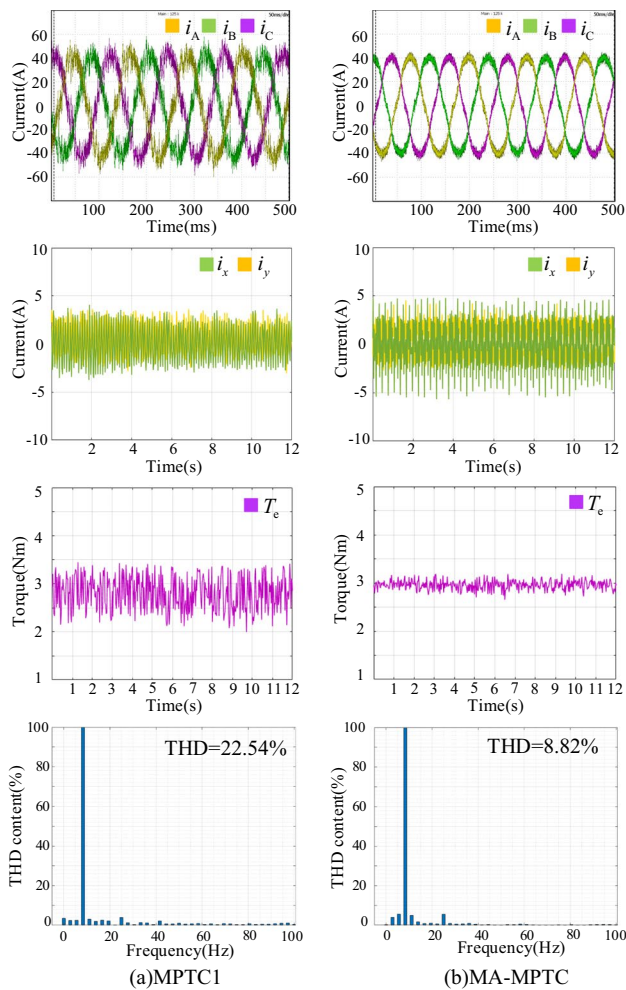


Fig. 9 Steady state performance at 100 rpm with a 3 N-m load: **a** MPTC1; **b** MA-MPTC (from top to bottom, the waveforms are the stator phase currents, harmonic currents, torque, and frequency spectra of the phase current i_A)

As can be seen in Figs. 9 and 10, the phase currents of the two methods are basically sinusoidal. However, the phase current waveform of MPTC1 is obviously distorted and fluctuates greatly. The phase current waveform of MA-MPTC is relatively smooth and fluctuates less. The total harmonic distortion (THD) analysis shows that the THD of MPTC1 is 22.54%, while MA-MPTC has a value of 8.82% at 100 rpm and a load of 3 N-m; and that the THD of MPTC1 is 13.88%, while MA-MPTC has a value of 6.71% at a load of 5 N-m. It can be observed that the THD is higher for small loads. Moreover, the THD of MPTC1 is much lower than that of MA-MPTC in both situations. Thus, the copper loss of the system is reduced.

Since both methods use VVVs to constrain the harmonic current component in the x - y subspace, their harmonic currents are kept small in the 10 A range. The set of candidate voltage vector of MPTC1 contains only VVVs. However,

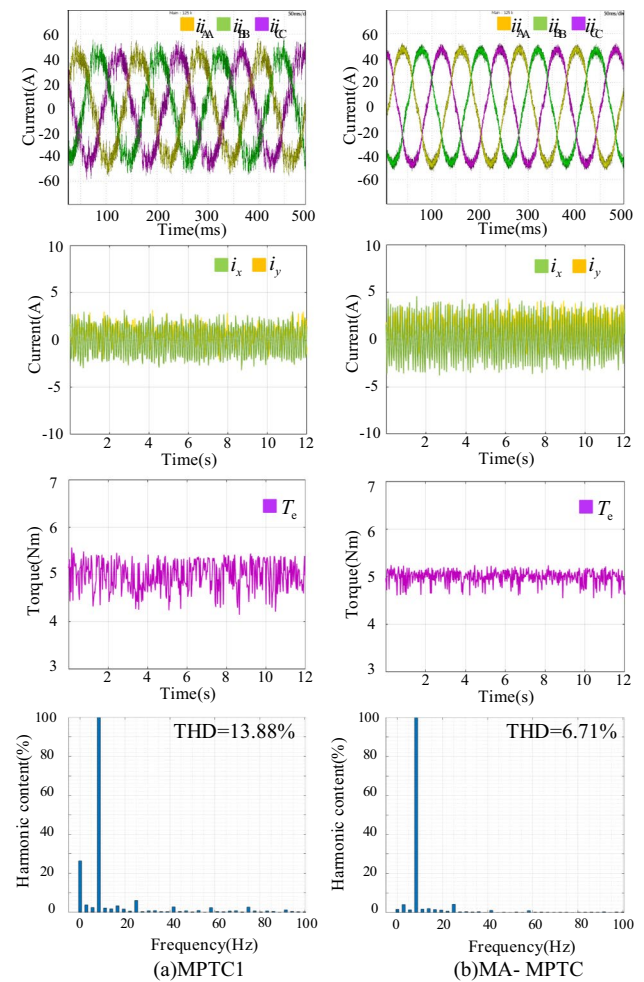


Fig. 10 Steady state performance at 100 rpm with a 5 N-m load: **a** MPTC1; **b** MA-MPTC

the set of candidate voltage vector of MA-MPTC consists of VVVs and the voltage vectors of groups L_3 and L_4 . The optimal vector selected by the cost function may belong to the L_3 group and L_4 group, which results in an increased harmonic current.

Therefore, the harmonic current of MPTC1 is slightly smaller than that of MA-MPTC.

In terms of torque tracking accuracy, MA-MPTC has significant advantages over MPTC1. Quantification of the experimental results gives the torque ripple values in Table.

Tables 2 and 3, which can be calculated according to (21). When the reference torque is 3 N-m, the torque ripples of

Table 2 Torque ripple at 100 rpm with 3 N-m

| | T_e^{ripple} | T_e^{ripple}/T_e^{ref} |
|---------|----------------|--------------------------|
| MPTC1 | 0.4235 N-m | 14.1167% |
| MA-MPTC | 0.1209 N-m | 4.03% |

Table 3 Torque ripple at 100 rpm with 5 N·m

| | T_e^{ripple} | $T_e^{\text{ripple}}/T_e^{\text{ref}}$ |
|---------|-----------------------|--|
| MPTC1 | 0.3103 N·m | 6.206% |
| MA-MPTC | 0.1527 N·m | 3.053% |

MPTC1 and MA-MPTC are 0.4235 N·m and 0.1209 N·m, respectively. In addition, the torque ripples of MPTC1 and MA-MPTC are 0.3103 N·m and 0.1527 N·m at a 5 N·m load.

$$T_e^{\text{ripple}} = \sqrt{\frac{1}{n} \sum_{i=1}^n (T_e - T_e^{\text{ref}})^2} \quad (21)$$

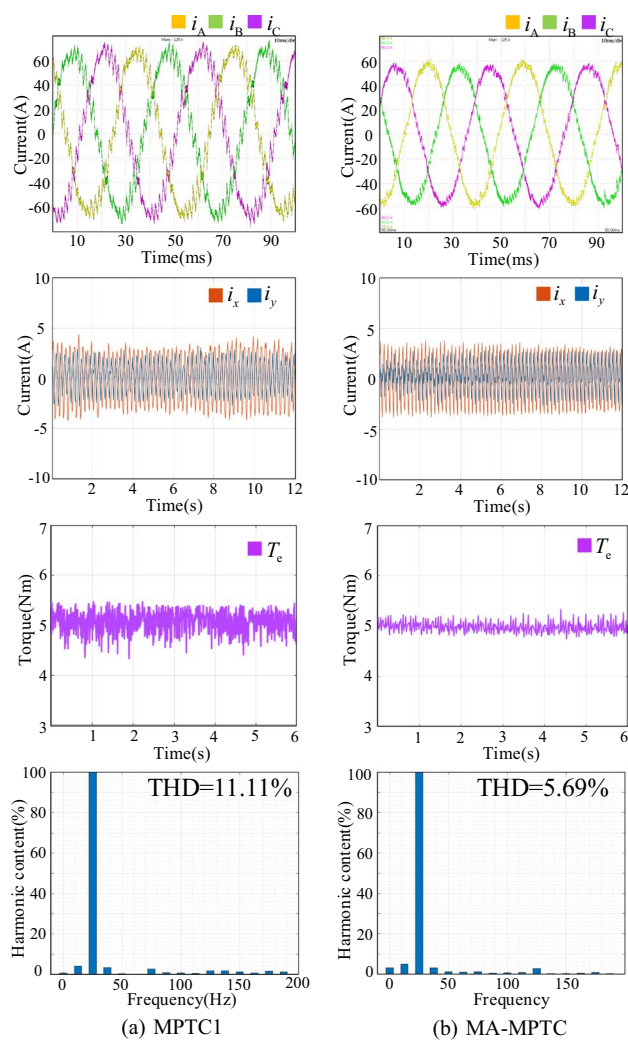
Obviously, the torque ripple of MA-MPTC is much smaller than that of MPTC1 under both load conditions. Since MPTC1 only applies CVVs with fixed amplitudes, the torque cannot be flexibly adjusted, which results in a large torque ripple. By constructing a vector set with multiple amplitudes, MA-MPTC can track the torque command more accurately and the torque ripple can be effectively suppressed.

In another test, the steady-state performance of a dual three-phase machine has been examined at its rated speed (300 rpm), as can be seen in Fig. 11. Similar performance can be observed when operating at 100 rpm. Thus, the proposed method achieves a much better phase current quality. Moreover, the THD at 300 rpm is slightly reduced.

when compared to the operation in Fig. 10. It can also be seen that the torque ripple of MA-MPTC is effectively reduced. This is because the candidate vectors with different magnitudes in MA-MPTC provide more flexibility when it comes to tracking the torque commands well. Therefore, the torque ripple is lower.

Finally, the dynamic performance can be seen in Fig. 12. In the experiment, the motor was initially controlled at 100 rpm under no-load and the load was suddenly changed to 3 N·m. Then the load torque was changed back to 0 N·m. As can be seen in Fig. 12, the torque command is tracked smoothly without overshoot during the transient process. Meanwhile, the greatly improved quality of the stator current can be observed in MA-MPTC. Moreover, a lower torque ripple is achieved by MA-MPTC. Additionally, when the motor reaches the steady state, the similar phase current performance with Fig. 9 can be observed.

The partial magnified view of the torque shows that the torque of the two MPTC methods can respond quickly to a sudden torque change. Both methods have similar response speeds. However, the torque performance of MA-MPTC is better, which is shown by lower torque ripple when compared with MPTC1. Therefore, the overall performance of the proposed MPTC is much better.

**Fig. 11** Steady state performance at 300 rpm with a 5 N·m load: **a** MPTC1; **b** MA-MPTC

6 Conclusion

In this paper, the MPTC method based on VVV was analyzed, and it was found that CVVs with a fixed amplitude led to a large torque ripple. Then this paper proposed a multi-amplitude CVV MPTC method that combines virtual and actual vectors. After the amplitude and position of the RVV were determined by a prediction method, three effective voltage vectors and one null vector located in the same sector as the RVV were selected as CVVs.

By designing a suitable cost function and evaluating the four CVVs, torque ripple was effectively suppressed. When compared with a MPTC method with VVVs, the torque ripple of MA-MPTC was shown to be reduced by more than 50%, while providing better torque control performance.

In addition, the computational cost was reduced by decreasing the number of CVVs. Moreover, the dynamic

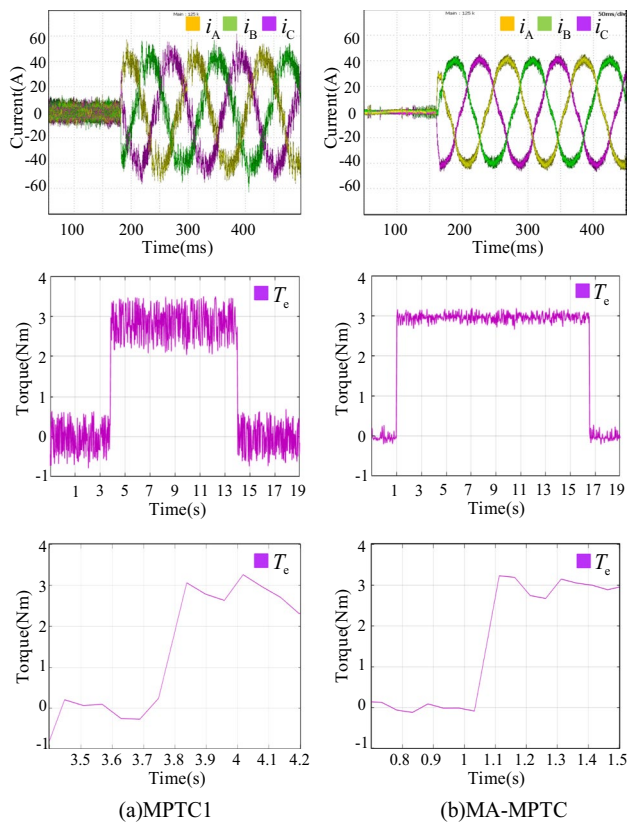


Fig. 12 Dynamic response during a sudden load change at 100 rpm: **a** MPTC1; **b** MA-MPTC

response times of both methods were kept within 100 ms, which means the fast dynamic response of the traditional MPTC method was maintained. Finally, experimental results confirmed the effectiveness of MA-MPTC.

The MPTC algorithm was based on motor parameters that can change in actual operation. Thus, the identification of motor parameters will be further considered in future research.

Funding Natural Science Foundation of Shanghai, 19ZR1418600, Shuang Wang.

Declarations

Conflict of interest On behalf of all authors, the corresponding author states that there is no conflict of interest.

References

1. Cervone, A., Slunjski, M., Levi, E., et al.: Optimal third-harmonic current injection for asymmetrical multiphase permanent magnet synchronous machines. *IEEE Trans. Ind. Electron.* **68**(4), 2772–2783 (2021)
2. Duran, M.J., Gonzalez-Prieto, I., Barrero, F., et al.: A simple braking method for six-phase induction motor drives with

- unidirectional power flow in the base-speed region. *IEEE Trans. Ind. Electron.* **64**(8), 6032–6041 (2017)
3. Nair, S.V., Harikrishnan, P., Hatua, K.: Six-step operation of a symmetric dual three-phase PMSM with minimal circulating currents for extended speed range in electric vehicles. *IEEE Trans. Ind. Electron.* **69**(8), 7651–7662 (2022)
4. Han, Y., Nie, Z., Xu, J., et al.: Mathematical model and vector control of a six-phase linear induction motor with the dynamic end effect. *J. Power Electron* **20**(3), 698–709 (2020)
5. Pandit, J.K., Aware, M.V., Nemade, R.V., et al.: Direct torque control scheme for a six-phase induction motor with reduced torque ripple. *IEEE Trans. Power Electron.* **32**(9), 7118–7129 (2017)
6. Fan, S., Tong, C.: Model predictive current control method for PMSM drives based on an improved prediction model. *J. Power Electron.* **20**(6), 1456–1466 (2020)
7. Aissa, O., Moulahoum, S.C., et al.: Analysis and experimental evaluation of shunt active power filter for power quality improvement based on predictive direct power control. *Environ. Sci. Pollut. Res.* **25**(25), 24548–24560 (2018)
8. N. Hamouda, B. Babes, S. Kahla, et al.: Predictive control of a grid connected PV system incorporating active power filter functionalities. 2019 1st International Conference on Sustainable Renewable Energy Systems and Applications (ICSRESA). 1–6 (2019)
9. Li, T., Sun, X., Lei, G., et al.: Finite-control-set model predictive control of permanent magnet synchronous motor drive systems—an overview. *IEEE/CAA J. Autom. Sin.* **9**(12), 2087–2105 (2022)
10. Zhou, C., Yang, G., Su, J.: PWM strategy with minimum harmonic distortion for dual three-phase permanent-magnet synchronous motor drives operating in the overmodulation region. *IEEE Trans. Power Electron.* **31**(2), 1367–1380 (2016)
11. Goncalves, P.F.C., Cruz, S.M.A., Mendes, A.M.S.: Disturbance observer based predictive current control of six-phase permanent magnet synchronous machines for the mitigation of steady-state errors and current harmonics. *IEEE Trans. Ind. Electron.* **69**(1), 130–140 (2022)
12. N. Hamouda, B. Babes, S. Kahla, et al.: Real time implementation of grid connected wind energy systems: predictive current controller. 2019 1st International Conference on Sustainable Renewable Energy Systems and Applications (ICSRESA). 1–6 (2019)
13. Luo, Y., Liu, C.: A simplified model predictive control for a dual three-phase PMSM with reduced harmonic currents. *IEEE Trans. Ind. Electron.* **65**(11), 9079–9089 (2018)
14. Gonzalez-Prieto, I., Duran, M.J., Aciego, J.J., et al.: Model predictive control of six-phase induction motor drives using virtual voltage vectors. *IEEE Trans. Ind. Electron.* **65**(1), 27–37 (2018)
15. Luo, Y., Liu, C.: Elimination of harmonic currents using a reference voltage vector based-model predictive control for a six-phase PMSM motor. *IEEE Trans. Power Electron.* **34**(7), 6960–6972 (2019)
16. Liu, S., Liu, C.: Virtual-vector-based robust predictive current control for dual three-phase PMSM. *IEEE Trans. Ind. Electron.* **68**(3), 2048–2058 (2021)
17. Ji, J., Jin, S., Zhao, W., et al.: Simplified three-vector-based model predictive direct power control for dual three-phase PMSG. *IEEE Trans. Energy Conversion* **37**(2), 1145–1155 (2022)
18. Agoro, S., Husain, I.: Model-free predictive current and disturbance rejection control of dual three-phase PMSM drives using optimal virtual vector modulation. *IEEE J. Emerg. Selected Top. Power Electron.* **11**(2), 1432–1443 (2022)
19. Ren, Y., Zhu, Z.Q.: Reduction of both harmonic current and torque ripple for dual three-phase permanent-magnet synchronous machine using modified switching-table-based direct torque control. *IEEE Trans. Ind. Electron.* **62**(11), 6671–6683 (2015)
20. Wang, W., Liu, C., Liu, S., et al.: Model predictive torque control for dual three-phase PMSMs with simplified deadbeat solution

and discrete space-vector modulation. *IEEE Trans. Energy Conversion.* **36**(2), 1491–1499 (2021)

21. Gu, M., Yang, Y., Fan, M., et al.: Finite control set model predictive torque control with reduced computation burden for PMSM based on discrete space vector modulation. *IEEE Trans. Energy Convers.* **38**(1), 703–712 (2022)
22. Yan, Y., Wang, S., Xia, C.L., et al.: Hybrid control set-model predictive control for field-oriented control of VSI-PMSM. *IEEE Trans. Energy Conversion.* **31**(4), 1622–1633 (2016)
23. Amiri, M., Milimonfared, J., Khaburi, D.A.: Predictive torque control implementation for induction motors based on discrete space vector modulation. *IEEE Trans. Ind. Electron.* **65**(9), 6881–6889 (2018)
24. Nikzad, M.R., Asaei, B., Ahmadi, S.O.: Discrete duty-cycle-control method for direct torque control of induction motor drives with model predictive solution. *IEEE Trans. Power Electron.* **3**(3), 2317–2329 (2018)
25. Vafaie, M.H., Dehkordi, B.M., Moallem, P., et al.: A new predictive direct torque control method for improving both steady-state and transient-state operations of the PMSM. *IEEE Trans. on Power Electron.* **31**(5), 3738–3753 (2016)
26. Wang, H., Zhao, W., Tang, H., et al.: Improved fault-tolerant model predictive torque control of five-phase PMSM by using deadbeat solution. *IEEE Trans. on Energy Conversion.* **37**(1), 210–219 (2022)
27. Li, X.L., Xue, Z.W., Zhang, L.X., et al.: A low-complexity three-vector-based model predictive torque control for SPMSM. *IEEE Trans. on Power Electron.* **36**(11), 13002–13012 (2021)
28. Guo, L., Zhang, K., Li, Y.: Double-voltage vector-based model predictive control for three-phase grid-connected ac/dc converters. *J. Power Electron.* **20**(1), 236–244 (2020)
29. Luo, Y., Liu, C.: Model predictive control for a six-phase PMSM motor with a reduced-dimension cost function. *IEEE Trans. Ind. Electron.* **67**(2), 969–979 (2020)
30. Yifan Zhao, T.A.: Lipo: Space vector PWM control of dual three-phase induction machine using vector space decomposition. *IEEE Trans. Ind. Electron.* **31**(5), 1100–1109 (1995)
31. Lee, J.S., Choi, C.H., Seok, J.K., et al.: Deadbeat-direct torque and flux control of interior permanent magnet synchronous machines with discrete time stator current and stator flux linkage observer. *IEEE Trans. Ind. Appl.* **47**(4), 1749–1758 (2011)
32. Wang, Y., Wang, X.C., Xie, W., et al.: Deadbeat model-predictive torque control with discrete space-vector modulation for PMSM drives. *IEEE Trans. Ind. Electron.* **64**(5), 3537–3547 (2017)

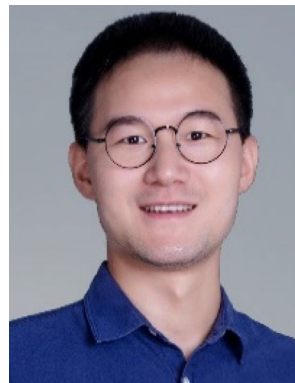
Springer Nature or its licensor (e.g. a society or other partner) holds exclusive rights to this article under a publishing agreement with the author(s) or other rightsholder(s); author self-archiving of the accepted manuscript version of this article is solely governed by the terms of such publishing agreement and applicable law.



Shuang Wang received his B.S., M.S., and Ph.D. degrees in Electrical Engineering from the Harbin Institute of Technology, Harbin, China, in 2000, 2005, and 2009, respectively. He is presently working as an assistant professor in the School of Mechatronic Engineering and Automation, Shanghai University, Shanghai, China. His current research interests include power electronics, sensors, and motor drives.



Qianru Zhang was born in 1998. She received her B.S. degree in Electrical Engineering from Shanghai University, Shanghai, China, in 2020, where she is presently working towards her M.S. degree in the School of Mechatronic Engineering and Automation. Her current research interests include motor drives and the control of permanent magnet synchronous motors.



Deliang Wu received his B.S. and Ph.D. degrees in Electrical Engineering from the Huazhong University of Science and Technology, Wuhan, China, in 2010 and 2015, respectively. From 2016 to 2018, he was a senior research engineer at Huawei Technologies Co., Ltd., China. In 2018, he joined Arizona State University, Tempe, Arizona, as a postdoctoral scholar. He joined Shanghai University, Shanghai, China, in 2020, where he is presently working as an associate professor. His current research interests

include wide band-gap power device applications and electric vehicle motor drives.



Jianfei Zhao received his B.S. and M.S. degrees in Mechatronic Engineering from Xi'an Jiaotong University, Xi'an, China, in 2000 and 2003, respectively. He received his Ph.D. degree in Electrical Engineering from Shanghai Jiaotong University, Shanghai, China, in 2012. He is presently working as an associate professor in School of Mechatronic Engineering and Automation, Shanghai University, Shanghai, China. His current research interests include power electronics and electronic

vehicles.